Flow Pattern and Turbulence Intensity in Stacks of Interrupted Parallel-Plate Surfaces

S. Mochizuki
Y. Yagi
Department of Mechanical Engineering, Tokyo University of Agriculture and Technology, Koganei, Tokyo, Japan

Wen-Jei Yang
Department of Mechanical Engineering and Applied Mechanics, The University of Michigan, Ann Arbor, Michigan

■An experimental study is performed to investigate the pressure drop distribution and turbulence intensity for airflow through a stack of parallel plates with periodic interruptions. The interrupted surfaces are constructed in an offset-strip form and a perforated form. Hot-wire measurements of the flow stream in the test core are made to determine turbulence intensity variations as a function of the Reynolds number. Results on the pressure drop and turbulence intensity are compared with those of the uninterrupted flow case. The offset-strip surface yields higher flow with higher turbulence intensity than the perforated and uninterrupted surfaces, an indication of superior heat transfer performance. Flow visualization by the dye injection method is performed on flow through a stack of offset-strip surfaces in a vertical water tunnel. Steady laminar flow, vortex shedding, oscillating flow, and turbulent flow are observed in sequence along the flow passage. The effects of Reynolds number on the location of the transition from steady to unsteady (oscillating and turbulent) flow regimes are determined. The study provides evidence to support the theory of secondary laminar-flow enhancement and transition-turbulent flow enhancement of heat transfer in compact heat exchangers [1–3].

Keywords: *augmentation, finned surfaces, flow instability, flow separation, flow visualization, forced convection, heat exchangers, measurement techniques, turbulence, wakes*

INTRODUCTION

In the plate-finned heat exchanger, which is the most important form of compact heat exchanger, interrupted surfaces are most commonly employed to enhance heat transfer performance by periodically disrupting the thermal boundary layer that develops on the heat transfer surface. Perforated, offset-strip, and louvered fins are typical examples of interrupted surfaces.

In addition to the Reynolds and Prandtl numbers, the flow and heat transfer characteristics of the interrupted surfaces in a heat exchangers core are affected by a large number of physical parameters related to the geometry of both the core and the heat transfer surface within the core. For example, Shah [4] counted 21 parameters affecting the heat transfer performance of a plate-finned type of heat exchanger with perforated surfaces. Furthermore, due to the presence of boundary layer separation and reattachment as well as vortex generation [5], the pressure drop and heat transfer mechanisms within the core are generally very complex. This is evidenced in a gas flow through a plate-finned heat exchanger with interrupted fins. Vortex shedding, which occurs in the wake of flow behind the fin edges, often excites acoustic modes of the duct, resulting in vigorous vibration accompanied by the generation of acute noise. The phenomenon is induced by the coupling of vortex shedding with acoustic resonance, which becomes very strong when the frequency of generated noise coincides with the natural frequency of vortex shedding.

Recently, efforts have been directed toward the understanding of heat transfer mechanisms through the disclosure of fundamental structures of the associated fluid flow. They have been confined to the investigation of flow in certain idealized model cores that simulate only a limited portion of the structures in actual heat exchangers. For example, one or two rows of interrupted parallel plates were aligned in the flow direction as a model to represent the unit with interrupted surfaces [6]. Obviously, flow phenomena were oversimplified in these studies, which were intended to provide information about the basic phenomena in each model. Sparrow and Hajiloo [7] measured the pressure drop for an array of staggered plates aligned parallel to an airflow but failed to investigate the details of flow behavior.

Theoretical studies that solved the conservation equations of mass, momentum, and heat for flow in the core models by means of large-scale digital computers were conducted. These investigations [eg, 8, 9] were limited to steady laminar flow cases. It is commonly observed in heat exchanger cores that even in the laminar regime the flow may be unsteady because of vortex shedding. In the case of high Reynolds number flow, the downstream region in the core is characterized by turbulent flow. Although numerical analysis by means of digital computers has a bright future as a method for investigation of the flow mechanisms in heat exchanger cores, it is currently neither well established nor reliable due to unusually complex flow phenomena.

Theory on three heat transfer enhancement mechanisms in compact heat exchangers was derived from performance correla-

Address correspondence to Professor Wen-Jei Yang, Department of Mechanical Engineering and Applied Mathematics, The University of Michigan, Ann Arbor, MI 48109.

Experimental Thermal and Fluid Science 1988; 1:51–57

0894-1777/88/$3.50

tions [1–3]. The three types are transition-turbulent flow enhancement, secondary laminar flow enhancement, and laminar flow enhancement. Evidence from flow structures in the heat exchanger cores is desired to shed light on the enhancement mechanisms.

The measurements of pressure-drop distribution and turbulence intensity in stacks of interrupted parallel-plate surfaces in a wind tunnel are conducted in the present study. Scale-up models are constructed in full compliance with actual heat exchangers. The interrupted surfaces include offset-strip fins and slotted fins. The geometrical parameters of these fins are varied to determine their effects on flow characteristics. The dye injection method was used to visualize the flow and determine the flow patterns in a model core in a vertical wind tunnel.

TEST CORES

For scale-up model testing of the plate-fin heat exchanger, 18 test cores with different fin geometries were fabricated for experiments in the present study. All test cores had basic structures similar to the one shown in Fig. 1, differing only in the patterns of fin arrangement. Fins and their base plates were made of 1.6 mm thick copper plates. The base plates were cut with slots into which the ends of the fins were inserted to form a test core. In every test core, ten static pressure holes were drilled in the base plate in the direction of airflow. Each static pressure was taken to the core exterior by means of a pressure tap.

Three types of interrupted heat transfer surfaces were fabricated and tested: plain straight fins (PSFs), offset-strip fins (OSFs), and slotted fins (SLFs). As illustrated in Fig. 2, offset-strip fins and slotted fins may be treated as plain straight fins with offsets and slots, respectively. A plain straight fin is periodically cut and offset at an interval c in the flow direction to form an offset-strip fin (Fig. 2*a*). In Fig. 2*b*, a slotted fin is made from a plain straight fin by cutting slots with gap s periodically at an interval l in the flow direction. Distance l is equal to $c + s$, where c is the fin length in the flow direction. All three types have the same transverse pitch a for convenience in comparing the performance characteristics of offset-strip and slotted fins with plain straight fins as the reference. In the present study, the basic dimension of the heat transfer surfaces such as a, b (plate spacing), and δ_f (fin thickness) together with the core size were fixed as shown in Table 1. Eighteen fins including one plain straight fin, five offset-strip fins, and 12 slotted fins were selected systematically in Table 1, and their test cores consisting of a single row were fabricated. The characteristic length of flow passages in the core is represented by the hydraulic diameter

$$d_h = 4A_c/S \tag{1}$$

Here, A_c and S denote the minimum cross-sectional area and wetted perimeter of airflow passages, respectively. In the case of an offset-strip fin, an average value was adopted for the core fronted area A_{fr}, since the fin numbers in the raw data counted 5 and 6 intermittently.

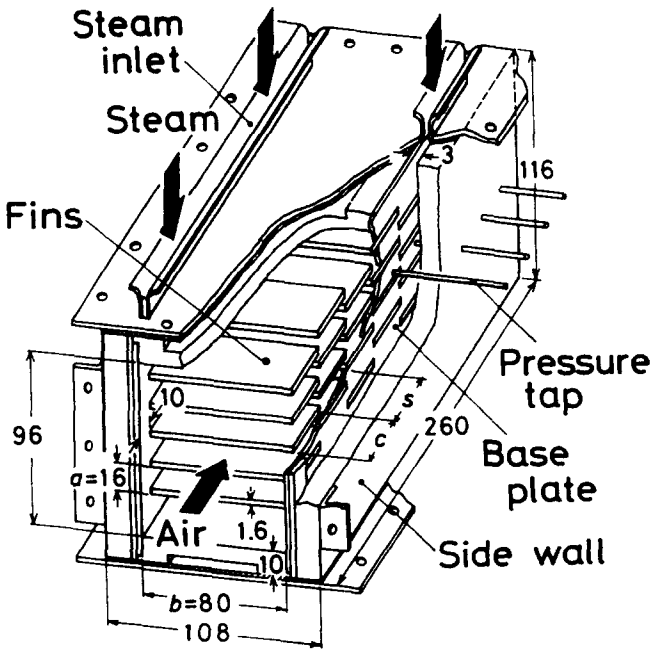

Figure 1. A schematic of a test core.

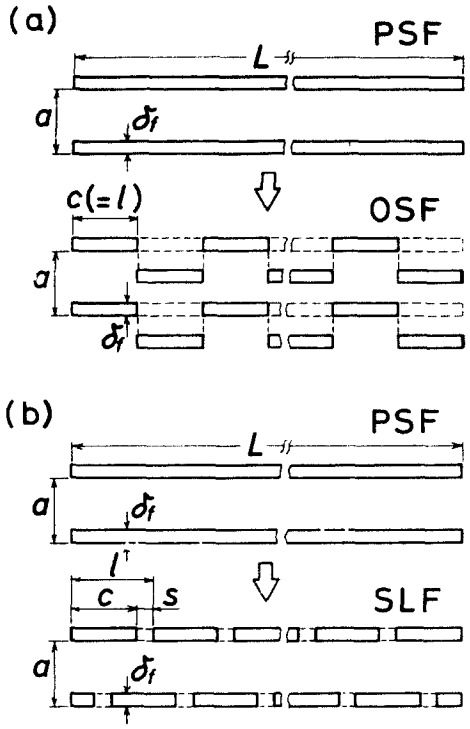

Figure 2. Construction of interrupted surfaces.

TEST APPARATUS AND PROCEDURE

Figure 3 depicts a schematic of the test apparatus. It consisted of a test section of 96 mm × 80 mm rectangular cross section installed in a suction-type wind tunnel. The airflow rate $\dot{m}$ was adjusted by varying the opening of a damper located in the exhaust port of an air blower, which is not shown. It was monitored by a traversing pitot tube and a manometer, both installed in a circular flow passage downstream from the test core. Two 1 mm I.D. static pressure ports, one 60 mm upstream and the other 60 mm downstream of the test core, were installed on a side wall of the wind tunnel. They were connected to a U-tube manometer for measuring the static pressure difference from which the pressure drop between the core inlet and exit was determined. In order to measure the static pressure distribution along the airflow inside the test core, ten 1 mm I.D. static pressure taps were installed on a

Table 1. Physical dimensions of test cores.

	PSF	OSF					SLF											
Core No.	*1*	*2*	*3*	*4*	*5*	*6*	*7*	*8*	*9*	*10*	*11*	*12*	*13*	*14*	*15*	*16*	*17*	*18*
$d_h \times 10^3$ m	24.4	23.1	23.7		23.1							24.4						
$a \times 10^3$ m									16									
$b \times 10^3$ m									80									
$c \times 10^3$ m	240	120	80	40	24	12			12						24			
$s \times 10^3$ m		----------					1.5	3.0	4.0	6.0	8.0	12.0	3.0	4.0	8.0	12.0	16.0	24.0
$\delta_f \times 10^3$ m									1.6									
L/d_h	9.84	10.4	10.1		10.4							9.84						
l/a	15.0	7.5	5.0	2.5	1.5	0.75	0.844	0.938	1.00	1.13	1.25	1.50	1.69	1.88	2.00	2.25	2.50	3.00
s/δ_f		----------					0.938	1.88	2.50	3.75	5.00	7.50	1.88	3.75	5.00	7.50	10.0	15.0
c/a	15.0	7.5	5.0	2.5	1.5	0.75			0.75						1.50			
c/l		----------					0.89	0.80	0.75	0.67	0.60	0.50	0.89	0.80	0.75	0.67	0.60	0.50
A_f m^2	0.193	0.214	0.209	0.220	0.225	0.239	0.185	0.170	0.159	0.141	0.126	0.109	0.176	0.164	0.152	0.135	0.123	0.102
$A_w \times 10^2$ m^2	4.22	4.19	4.20		4.19		4.28	4.31	4.33	4.36	4.39	4.42	4.28	4.30	4.32	4.36	4.38	4.42
A m^2	0.236	0.256	0.251	0.262	0.267	0.281	0.228	0.213	0.202	0.185	0.170	0.153	0.219	0.207	0.195	0.179	0.167	0.147
$A_c \times 10^3$ m^2	1.15			1.14								1.15						
$\sigma = A_c/A_{fr}$	0.917	9.908	0.911		0.908							0.817						

side wall of the test core (Fig. 2). A rotary cock was employed to select and connect two ports to a manometer for pressure-difference readings (Fig. 3).

Three hot-wire probes were inserted into the test core through a base plate (not shown). They were installed at three different locations along the airflow: upstream, midstream, and downstream. Each probe was situated at the center between two adjacent fins and between the base plates.

A flow visualization study was conducted on an offset-strip fin in a vertical water tunnel of 60 mm × 50 mm cross section. The pattern of fin arrangement in the test core was geometrically similar to that of test core No. 6 in the wind tunnel tests, except for the aspect ratios of their flow cross sections. In other words, the two cores had identical magnitudes a/δ_f and c/δ_f of 10.0 and 7.5, respectively. However, the flow visualization core had the aspect ratio a/b of 0.4 with 18 fins, while core No. 6 had a/b of 0.2 and 20 fins. The dye injection method was adopted for visualizing the flow inside the test core.

RESULTS AND DISCUSSION

The static pressure distribution and the variations in turbulence intensity and Reynolds number along the airflow were determined. Results are depicted in Figs. 4–6.

Figures 4 and 5 show the static pressure distributions. The abscissa represents the dimensionless distance from the core entrance, x/L, while the ordinate represents the dimensionless static pressure drop from the entrance (P_1) to the location x(P_x), $\Delta P_x/P_0$. Here, L denotes the core length;

$$\Delta P_x = P_1 - P_x \tag{2}$$

and P_0 is standard atmospheric pressure of 1.013×10^5 Pa. The fin arrangement and the location of pressure taps (solid circles) in each core are also shown in the figures.

Figure 4 illustrates the static pressure distributions in a plain straight fin (core No. 1) and offset-strip fins (cores 2–6). In the case of the plain fin, the pressure-drop gradient was maximum near the core inlet $x/L = 0$ and diminished along the flow, because the hydrodynamic boundary layer continued to develop from the entrance. This clearly demonstrated the characteristics of pressure drop within the entrance region. In contrast, offset-strip fins (for example, core 2 or 3) had an abrupt pressure change at every interval between two adjacent fins due to the disruption of the boundary layers. Since the continuous development of the boundary layer is not allowed in an offset-strip fin, the shorter the fin length (consequently the greater the number of boundary layer separations), the stronger the pressure drop, which is attributed to the increase in both the form drag and frictional resistance. It results in a sharp increase in the pressure drop across the test core in the order of reducing c/a as observed in OSF cores 2–6, Fig. 4. In the cores with short fins such as cores 4–6, the pressure drop increases almost linearly along the flow. This implies that heat exchangers with short offset fins undergo a pressure drop of a magnitude linearly proportional to the core length L. It also means that the friction coefficient of offset-strip fins depends weakly on the ratio of core length to hydraulic diameter, L/d_h.

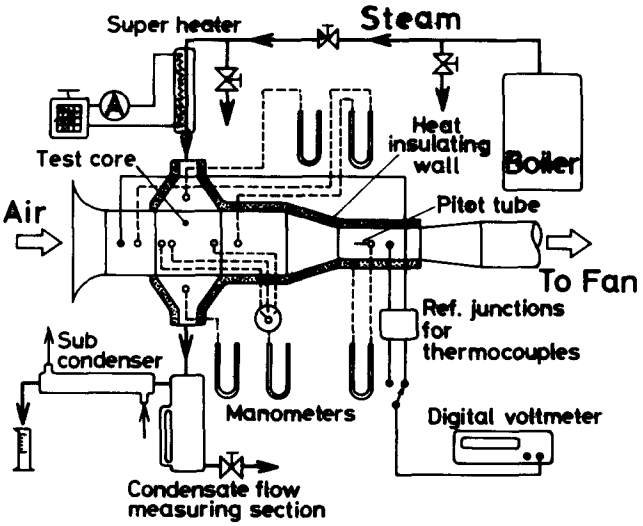

Figure 3. A schematic of experimental apparatus.

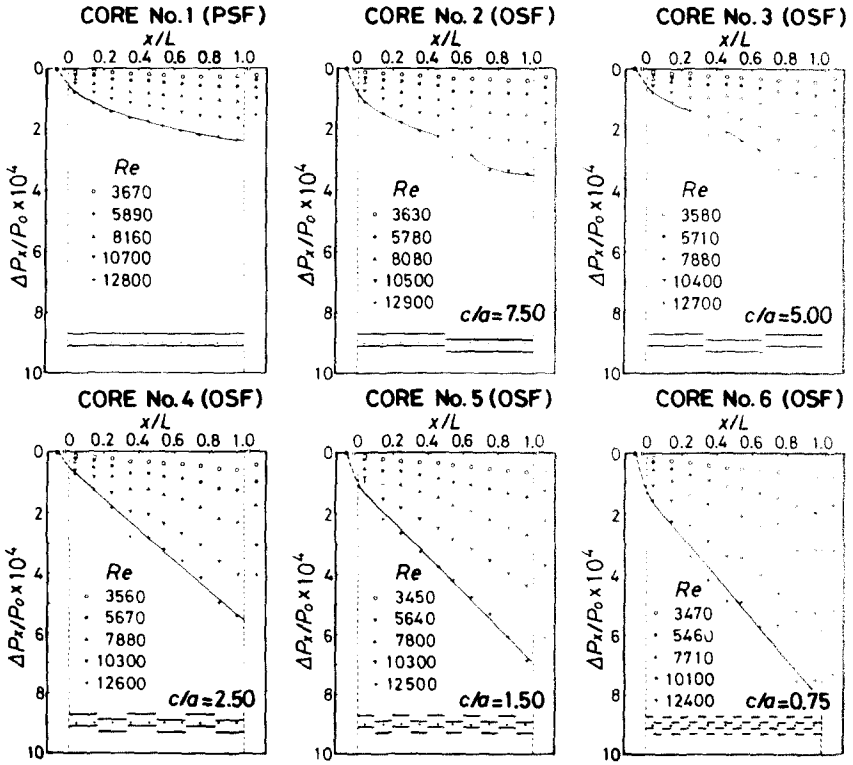

Figure 4. Static pressure distribution in PSF and OSF cores.

Figure 5 shows the results for a slotted fin with $c/a = 1.5$. When the slot width s/δ_f is small, it becomes difficult for boundary layer separation to occur at the downstream edges of the fins. This is shown in a comparison of SLF core No. 13 and PSF core No. 1: Their pressure drop performances are seen to be almost identical in both magnitude and tendency even at higher Reynolds numbers. As the slot width s/δ_f is increased, the pressure drop across the test core increases gradually (as in cores 14–16), reaching a maximum at $s/\delta_f = 7.5$ (core 16), then gradually diminishing (cores 17 and 18) to become lower (core

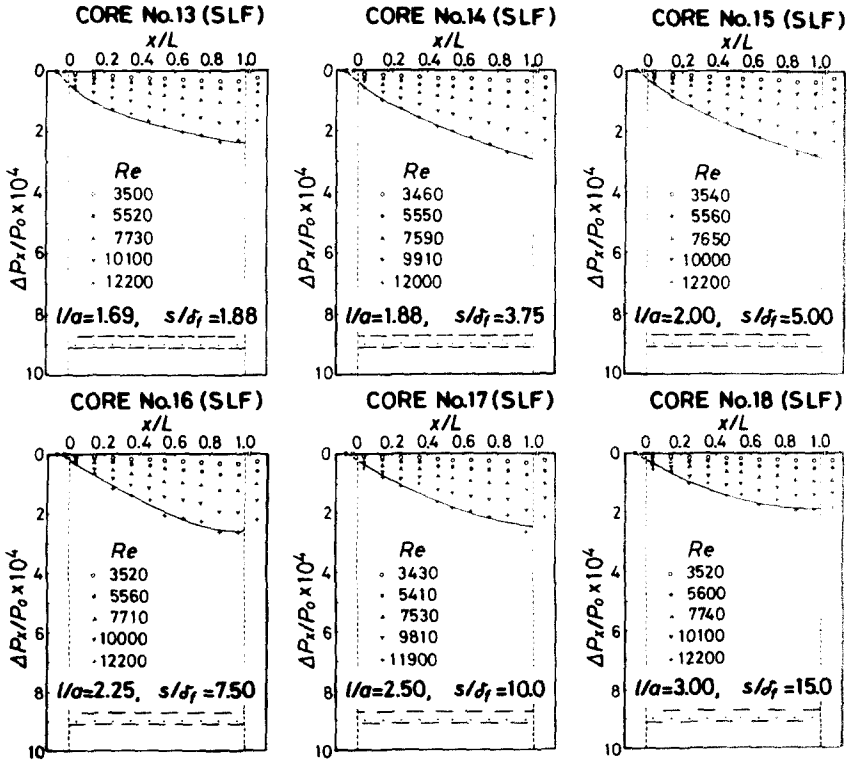

Figure 5. Static pressure distribution in SLF cores with $c/a = 1.5$.

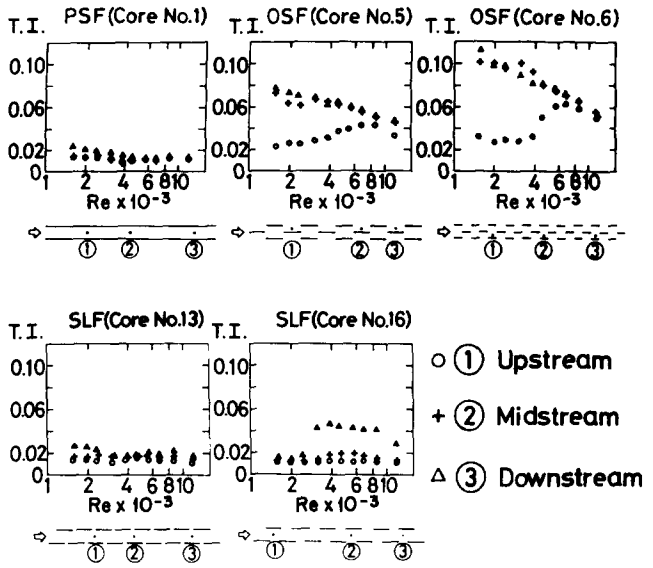

Figure 6. Turbulence intensity versus Re $\times 10^{-3}$ at upstream, midstream, and downstream points in PSF, OSF, and SLF cores.

18) than that of a plain straight fin. This tendency was also detected in the case of slotted fins (cores 7–12) with $c/a = 0.75$, which is not shown. The reason for SLF cores to experience such a feature in pressure-drop performance can be explained as follows. Even though the mixing effects due to flow separation from every fin are enhanced with an increase in s/δ_f, the combined effect of the number of surface disruptions (ie, number of fins or number of boundary layer separations) and the magnitude of the pertinent area (wetted surface area) begins to diminish when s/δ_f exceeds a certain value. It is disclosed by comparing Figs. 4 and 5 that no matter how the magnitude of s/δ_f is changed, the pressure drop in the SLF cores cannot be varied as much as the pressure-drop variations in the OSF cores.

In all cores in Figs. 4 and 5, one observes the pressure drop and rise at the core entrance and exit, respectively, undergoing abrupt changes. These are caused by a sudden reduction and a sudden enlargement in the flow cross-sectional area due to the finite thickness of the fins.

Figure 6 depicts the relationship between turbulence intensity TI and Reynolds number Re, where

$$\mathrm{TI} = (\overline{U'^2}/U_m)^{1/2} \tag{3}$$

$\overline{U'^2}$ represents the rms value of velocity variations and U_m is the mean flow velocity inside the test core. Hot-wire measurements were made at upstream, midstream, and downstream locations. The measurement location and fin arrangement for each core are also illustrated in Fig. 6. Due to the arrangement of the hot wires, their measurements reveal the variations in turbulent intensity along the flow that reflect the change in flow behavior.

The plain straight fin (core 1) has lower turbulence intensities (0.01–0.02) irrespective of the Reynolds number and measurement location. In other words, the flow was quiet (at low turbulence intensity) throughout the core. In contrast, the OSF cores, for example Nos. 5 and 6, had turbulence patterns significantly different from those of the PSF:

1. At low Reynolds numbers, the flow was quiet upstream but had high turbulence intensities at midstream and downstream regions.
2. As the Reynolds number was increased, the turbulence intensity was gradually amplified upstream but was gradually damped at midstream and downstream regions.
3. As the Reynolds number reached a sufficiently high value, the turbulent intensity became nearly uniform throughout the core. Its magnitudes were much higher than those in the PSF core. The smaller the fin length c was, the higher would be the turbulence intensity, as seen by comparing the OSF cores 5 and 6.

Measured results of cores 13 and 16 are illustrated in Fig. 6 as representative examples of slotted fins. They had identical fin lengths $c/a = 1.5$ but different slot widths s/a. It is revealed that:

1. In the case of small slot width (core 13), turbulence intensity was not influenced by the presence of slots and was almost identical to the PSF core. This means that turbulence intensity was low throughout the core, irrespective of Reynolds number.
2. Even with a large slot width (core 16), low turbulence intensity prevailed throughout the core at low Reynolds numbers. As Re was increased, turbulence intensity was enhanced only in the downstream region, remaining low in the upstream and midstream sections irrespective of the Re value. In other words, the SLF core can have a higher turbulence intensity than the PSF core only in the downstream region at high Re and large slot width. Generally, the effect of fin arrangement on flow turbulence is smaller in the SLF core than in the OSF core.

In conclusion, plain straight, offset-strip, and slotted fins have their own characteristics of turbulence intensity which are intimately related to the flow situation within the core. It is therefore desirable to enhance the entire image of the flow situation within the core by flow visualization techniques.

It should be noted that the uncertainties in pressure drop and turbulent intensity were estimated to be about $\pm 12\%$ and $\pm 8\%$, respectively.

An example of the flow visualized within the OSF core is depicted in Fig. 7. It is observed that:

1. When Re is low, steady laminar flow patterns prevailed throughout the core, not shown.
2. As Re is increased, the von Karman vortices shed from each fin produced periodic fluctuations in the core flow in the downstream region. The uppermost location for shedding of such vortices, as seen in Figs. 7*a* and *b*, gradually shifted upstream with an increase in Re. Downstream there was a periodically oscillating flow of large amplitudes, whereas steady laminar flow existed in the upstream region from the vortex-shedding site.
3. When Re grew higher, the vortex-shedding site migrated further upstream, and vortex generation could be observed at the first row of fin arrangement, as seen in Figs. 7*c* and *d*. Immediately downstream there was a periodically oscillating flow, and thereafter a turbulent flow with violent mixing. In this case, steady laminar flow occupied only a length of the first fin row, while the major part of the core was dominated by periodically oscillating flow and turbulent flow. One observes that steady laminar, periodically oscillating, and turbulent flow coexist sequentially along the flow. However, the transition from one flow regime to the succeeding one is so gradual that a distinct transition Reynolds number cannot be determined.

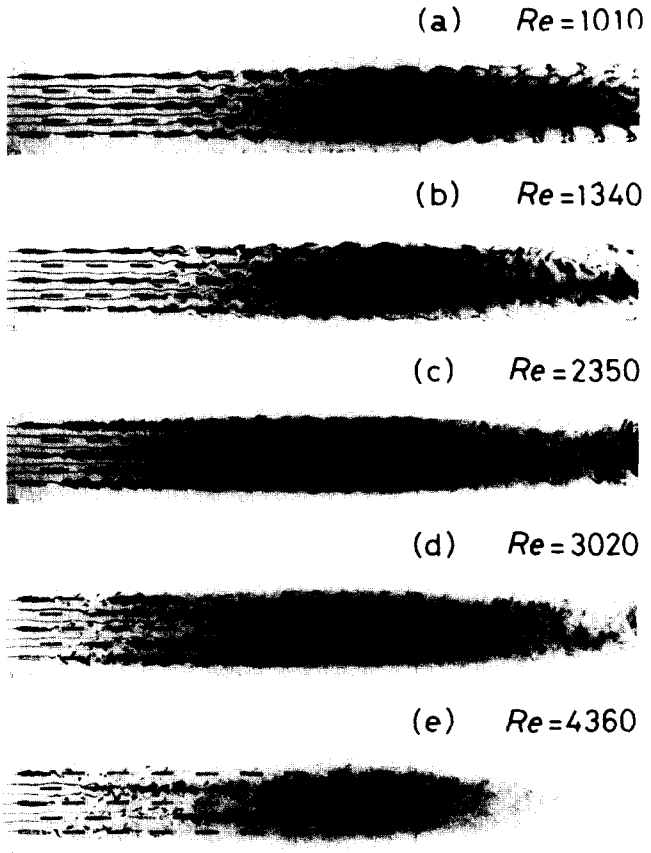

Figure 7. Flow patterns in OSF cores at various Reynolds numbers.

4. If Re was increased further, turbulent flow was extended to seize most of the core space, as shown in Fig. 7*e*.

It is concluded that the region of strong turbulence migrates upstream with an increase in Reynolds number. This observation can explain the mechanism for the variation of turbulence intensities in OSF core 6 with both the location along the flow and the magnitude of Re.

CONCLUSIONS

An experimental study has been conducted to determine the flow pattern and turbulence intensity in the scale-up model cores of representative interrupted surfaces such as offset-strip fins and slotted fins. In their basic structure, the model cores resemble actual compact heat exchangers. It is concluded from the study that:

1. For offset-strip fins with the hydrodynamic boundary layer being prevented from continuous development, the shorter the fin length (accordingly, the more frequent the boundary layer separations), the faster the drop in pressure across the core.
2. In the OSF core with short fins, static pressure falls almost linearly along the flow. Hence, the pressure loss in the OSF type of heat exchanger is approximately proportional to the flow length L.
3. The pressure-loss characteristics in the SLF core with small slot width have the same magnitude and tendency as those in the PSF core irrespective of Re. When the slot width is increased, the pressure drop across the core increases, reaches a maximum value, and then decreases gradually. It may be reduced to a value even lower than that in the PSF core.
4. Turbulence intensity in the OSF core varies significantly with the location in the flow direction, Re, and fin length. At low Re values, turbulence intensity may be low in the upstream region but is generally quite high elsewhere in the core. When Re is large, the strength of turbulence intensity is approximately uniform throughout the core.
5. The shorter the fin length, the higher the turbulence intensity in the OSF core.
6. The turbulence intensity in the SLF core is little influenced by the location along the flow direction, Re value, and fin length. It is higher than that in the PSF core only in the downstream region when both the slot width and Re are large.

It is concluded that the OSF core has higher turbulence intensity and consequently would result in higher heat transfer performance than the SLF and PSF cores. At low Re, steady laminar flow prevails throughout the entire OSF core. As Re is increased, oscillating flow appears downstream of steady laminar flow, resulting in the secondary laminar flow enhancement of heat transfer performance [1–3]. At high Re, steady laminar, oscillating, and turbulent flow appear in sequence along the flow. The turbulent flow region spreads upstream with an increase in Re and may eventually occupy the entire flow passage in the OSF core. The dominance of the flow passage by turbulent flow causes the occurrence of a transition-turbulent flow enhancement mechanism in heat transfer inside compact heat exchangers [1].

One should note that flow patterns may change significantly between the core inlet and the exit and the extent of each flow pattern within the core may vary with Re. If a model core is to be used in determining the flow patterns in an actual heat exchanger, the model must be equipped with an appropriate number of rows of fins in the flow direction to match the actual unit. In other words, a model core with only a few rows of fins cannot properly represent an actual unit with a large number of rows of fins.

NOMENCLATURE

A	heat transfer area, m^2
A_c	minimum flow cross-sectional area inside core, m^2
A_{fr}	core frontal area, m^2
A_w	wall surface area, m^2
a	transverse pitch of fins, m
b	plate spacing, m
C_p	specific heat of air, kJ/(kg K)
c	fin length, m
d_h	hydraulic diameter, m
L	fin length in flow direction, m
l	longitudinal pitch of fin, m; $l = c$ for offset-strip fins; $l = c + s$ for slotted fins
P_0	atmospheric pressure, N/m^2
P_1	static pressure at core entrance, N/m^2
P_x	local static pressure inside core, N/m^2
ΔP_x	$P_1 - P_x$, N/m^2
Re	Reynolds number ($= U_m d_h/\nu_m$), dimensionless
S	wetted perimeter, m
s	slot length in flow direction for slotted fins, m
U_m	mean velocity inside core ($= \dot{m}/\rho_m A_c$), m/s

$\tilde{U}'$ fluctuating component of flow velocity, m/s

x distance along the flow measured from core inlet, m

Greek Symbols

δ_f plate thickness, m

Abbreviations

OSF offset-strip fin

PSF plain straight fin

SLF slotted fin

REFERENCES

1. Yang, W.-J., Three Kinds of Heat Transfer Augmentation in Perforated Surfaces, *Lett. Heat Mass Transfer,* **5**, 1-10, 1978.
2. Lee, C. P., and Yang, W.-J., Augmentation of Convective Heat Transfer from High-Porosity Perforated Surfaces, *Heat Transfer 1987.*
3. Yang, W.-J., Forced Convective Heat Transfer in Interrupted Compact Surfaces, *Proc. 1983 ASME-JSME Thermal Engineering Joint Conf.,* 105-111, 1983.
4. Shah, R. K., Perforated Heat Exchanger Surfaces, Part 2. Heat Transfer and Flow Friction Characteristics, ASME Paper 75-WA/HT-9, 1975.
5. Mochizuki, S., and Yagi, Y., Characteristics of Vortex Shedding in Plate Arrays, *Flow Visualization II,* W. Merzkirch, Ed., Hemisphere, Washington, DC, pp. 99-103, 1982.
6. Cur, N., and Sparrow, E. M., Experiments on Heat Transfer and Pressure Drop for a Pair of Collinear, Interrupted Plates aligned with the Flow, *Int. J. Heat Mass Transfer,* **21**, 1069-1080, 1978.
7. Sparrow, E. M., and Hajiloo, A., Measurements of Heat Transfer and Pressure Drop for an Array of Staggered Plates Aligned Parallel to an Air Flow, *J. Heat Transfer,* **102**, 426-432, 1980.
8. Suzuki, K., Hirata, E., Miyake, T., and Sato, T., Numerical and Experimental Studies on a Two-Dimensional Model of an Offset-Strip-Fin Type Compact Heat Exchanger used at Low Reynolds Number, *Int. J. Heat Mass Transfer,* **28**, 823-836, 1985.
9. Sparrow, E. M., Baliga, B. R., and Patankar, S. V., Heat Transfer and Fluid Flow Analysis of Interrupted-Wall Channels, with Application to Heat Exchangers, *J. Heat Transfer,* **99**, 4-11, 1977.